Journal of Marine Research, 66, 873–898, 2008

Energetics in Delaware Bay: Comparison of two box models with observations

by Ana E. Rice[1,2], Michael M. Whitney[3], Richard W. Garvine[1,4] and Pablo Huq[1]

ABSTRACT

A corrected version of an unstratified box model of potential energy anomaly ϕ, initially developed by Garvine and Whitney (2006), and a new two-layer box model that allows for stratified and well-mixed conditions are applied to Delaware Bay. The models are applied for the Garvine and Whitney (2006) 1988-1994 study period and in Spring 2003; however, only model results of potential energy anomaly from the latter period are compared to *in situ* observations obtained outside the bay mouth. Unstratified model results for the two study periods reveal that the river discharge (Ω_1) is the largest potential energy anomaly contributor. This term is closely followed (but with opposite sign) by the coastal current efflux term (Ω_2). For the two-layer model the largest contributor is the dense inflow term (Ω_6). The wind term (Ω_5) is the second largest, followed by the tide (Ω_3), river discharge (Ω_1) and coastal current terms. In both models the solar heat flux term (Ω_4) makes the smallest contribution to ϕ. The available one-month comparison of model results to observations renders statistically insignificant correlation coefficients for both models. We speculate dynamical differences between conditions at the estuary mouth and the instrument location on the nearby shelf contribute to the model-observation mismatch. Other statistics, such as the root mean square error indicate that the unstratified model performs better than the two-layer model for the observation period. The latter model is, however, able to depict the importance of tides and winds in the computation of potential energy anomaly and is able to detect the response of ϕ due to strong wind events. While there is no clear model choice for the Delaware Bay, the unstratified model may be entirely inappropriate for highly stratified estuaries.

1. Introduction

It is important to understand the mixing and exchange processes that occur between estuarine waters and the coastal ocean as these systems provide major gateways for the transfer of materials from continents to the ocean (Henrichs *et al.*, 2000). A viable approach for studying mixing processes is through the computation of available potential energy, ϕ (J m^{-3}), defined as the energy stored within the system that has the 'potential' to change the state of the dynamics in the system when the energy is released (Serway and Jewett, 2004).

1. College of Marine and Earth Studies, University of Delaware, Newark, Delaware 19716, U.S.A.
2. Corresponding author. ***email: eguiluz@udel.edu***
3. Department of Marine Sciences, University of Connecticut, Groton, Connecticut, 06340, U.S.A.
4. Deceased.

Simpson and Hunter (1974) pioneered the use of potential energy anomaly when studying sea fronts in the Irish Sea and then applied ϕ to study the development and breakdown of stratification from river discharge in estuaries (e.g. Simpson *et al.*, 1990; 1991; and Simpson and Bowers, 1981). Recently, Garvine and Whitney (2006) (from now on GW06), noted that the ratio of kinetic to potential energy (or the internal Froude number squared) in the delivery of riverine freshwater through the estuary and adjacent shelf is typically small compared to unity. The authors therefore concluded that the bulk of the energy content associated with buoyant river discharge is in the form of potential energy.

Box models for the study of dynamical processes are attractive due to their simple nature and relatively straightforward application. Generally, box models are applied to physical systems to model complicated dynamics from simplified inputs and model characteristics. These models therefore serve as low-level interpretive and/or predictive tools, providing users with a simplified physical picture of the system. A recent example of a box model application is found in GW06. In that paper, the authors draw on the box models of Stommel (1961), Hamilton *et al.* (1985) and Austin (2002) for inspiration in an attempt to accurately represent the dynamics in the coastal boundary conditions of climate models. They assess the freshwater delivery to the Delaware shelf and deep ocean by developing a coupled box model of the Delaware Bay estuary and shelf. The estuarine component of the model assumes an unstratified water column; it computes the potential energy anomaly budget in the estuary domain and the potential energy flux to the shelf. The authors compare box model results of freshwater flux to observations, and potential energy anomaly box model results to ϕ results from the primitive equation hydrodynamic three-dimensional Estuarine, Coastal and Ocean model (ECOM3D). Their work, however, does not compare model potential energy anomaly to *in situ* ϕ data. In an attempt to understand mixing dynamics of the region and to assess model performance, the present study employs a corrected version of the potential energy anomaly box model of GW06 in the Delaware estuary. In addition, we develop a two-layer box model that allows for mixing and stratification in the estuary. The models are run for the GW06 study period and the Spring of 2003. For the latter period model results are compared to available *in situ* observations obtained from the Delaware Circulation and Dye Experiment (DECADE), which was undertaken to study mixing and circulation processes between Delaware Bay and the coastal ocean via the Delaware coastal current (DCC).

Many aspects of the dynamics of the Delaware Bay buoyant outflow have been elucidated by Garvine and co-workers. For example, the role of buoyancy and wind-forcing in the dynamics and the variability of the vertical structure of the buoyant plume were resolved by Münchow and Garvine (1993 a,b) and Wong (1998). The classification scheme of Garvine (1995) showed that the Delaware Bay buoyant outflow was a large-scale weakly nonlinear outflow. Sanders and Garvine (2001) found that the freshwater delivery is controlled primarily by upland freshwater discharge into the estuary and along-estuary winds, and that during upwelling-favorable winds, the plume at the surface tends to spread offshore, whereas

during downwelling-favorable winds it is confined to the coast. Incorporation of realistic wind conditions, tidal fluctuations and river discharge in simulations of the Delaware Bay buoyant outflow using ECOM3D was successfully undertaken by Whitney and Garvine (2005; 2006).

The field portion of DECADE took place in the Spring of 2003 and 2004 on the continental shelf in the vicinity of the Delaware Bay mouth. A mooring array was deployed each year. The purpose of the mooring deployment was to obtain vertical profiles of salinity, temperature and velocity, so the moorings were designed to be of the U-shape type composed of a slack wire, ground wire and taut wire. Each slack wire contained an S4 current meter (equipped with temperature and salinity sensors) at 2-m depth, followed by 8 thermistors. On the taut wire, an S4 meter was placed at 6-m depth, followed by three CT sensors. Density was computed at the moorings only for the CT sensors and S4 current meters, so regression analysis was employed to infer the density field from temperature. From the analysis, 15-minute density data (with a typical vertical spacing of 2 m) were obtained. Out of the six moorings deployed in DECADE, mooring DC (deployed on the 18-m isobath; see Fig. 1) was closest to the bay mouth and so its data are analyzed in this study for comparison

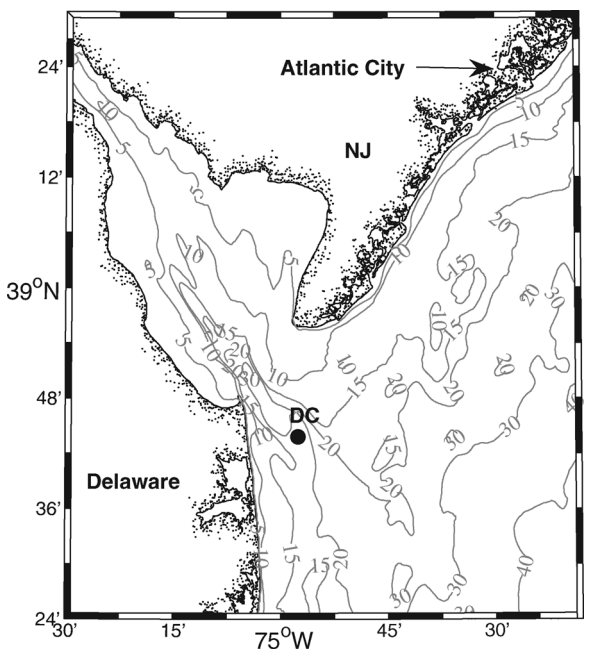

Figure 1. Study area for the Delaware Circulation and Dye Experiment (DECADE). Density data was obtained from mooring DC and wind data from Atlantic City, NJ. Depth contours are depicted in meters.

to box model results. Due to poor data resolution in the top half of the water column at the mooring in 2004, only data from the Spring of 2003 (April 10 to May 10) are examined.

This paper is divided into five sections. In Section 2 the potential energy anomaly is defined and a corrected version of the GW06 unstratified box model is summarized. In addition, a two-layer box model case is developed to allow for stratified and well-mixed conditions in the estuary. In Section 3 the corrected unstratified and two-layer models are applied to the Delaware Bay for the GW06 study period. Mixing dynamics are inferred from the annual signals and results from the two box models are compared. In Section 4, ϕ is computed from density observations at mooring DC in the Spring of 2003. Mixing dynamics are analyzed and potential energy anomaly results are compared to unstratified and two-layer model results of the Delaware Bay for the study period. The summary and conclusions follow in Section 5.

2. Potential energy estuarine box model

a. Potential energy anomaly

The potential energy anomaly definition used in GW06 was modified from the original definition (e.g. Simpson *et al*., 1990) in order to account for all estuarine potential energy inputs to the shelf. The original definition is the local potential energy anomaly of the water column (relative to the free surface):

$$\phi_{local} = \frac{g}{h}\int_{-h}^{0}(\overline{\rho} - \rho)\, z dz \tag{1}$$

i.e. where z is the vertical coordinate (positive upward), h is depth, g is gravitational acceleration, $\overline{\rho}$ is the depth-averaged density, and ρ is the potential density through the water column. This ϕ_{local} increases with increasing stratification, decreases due to vertical mixing, and reaches zero for a well-mixed water column.

The original definition does not include all the potential energy inputs that estuaries contribute to the shelf. For instance, a vertically well-mixed estuary has $\phi_{local} = 0$ even though its lower densities introduce a significant buoyancy source to the shelf. Consequently, GW06 used a modified potential energy anomaly for box model formulation (ρ_s is the shelf reference density):

$$\phi = -\frac{g}{h}\int_{-h}^{0}(\rho_s - \rho)\, z dz. \tag{2}$$

This potential energy anomaly can be separated into two contributions: $\phi = gh(\rho_s - \overline{\rho})/2 - \phi_{local}$. The first contribution (ϕ_1) will be positive for any typical estuary. This contribution increases as depth-averaged densities decrease due to freshwater inflow or surface heating; while it decreases due to dense water inflows through the mouth. The increased stratification caused by these factors causes the second contribution ($-\phi_{local}$) to grow more negative; competing with the positive first term. Vertical mixing from tides and winds decreases stratification but cannot affect depth-averaged densities directly. Consequently,

vertical mixing increases ϕ due to changes only in $-\phi_{local}$. Any estuary that has a maximum density not exceeding ρ_s and a stably stratified or well-mixed water column will have positive ϕ values at all times.

b. Model formulation

The coupled box model developed by GW06 is composed of an estuarine box and a shelf box whereby river water flows into the estuarine box and mixed freshwater and coastal water are output from the shelf box to the deep ocean (GW06). For the purpose of their study and herein only the estuarine box model is discussed and tested.

Our goal is to assess the time rate of change of the potential energy anomaly in the estuary from fluxes across the boundaries, both vertical and horizontal and from interior processes. In the estuarine box model, ϕ can vary in response to competing rates of change associated with riverine freshwater inflow (Ω_1), mixed water outflow to the shelf (Ω_2), tidal mixing (Ω_3), surface heat flux (Ω_4), wind-induced mixing (Ω_5), and dense-water inflow (Ω_6). The equation expressing the budget of the area-averaged potential energy anomaly in the estuary (ϕ_e) is:

$$a A_e \frac{d\phi_e}{dt} = \sum_{i=1}^{N} \Omega_i \tag{3}$$

where A_e is the total surface area of the estuary and a is the surface area fraction covered by the estuary box. Table 1 lists the expressions for the potential energy anomaly rate components (Ω_i) for the unstratified and two-layer cases and Table 2 lists variables associated with Ω_i.

In order to obtain a solution, additional information is needed: ϕ_e must be defined in terms of the estuary-averaged density (ρ_e), the outflowing density at the mouth (ρ_m) must be linked to ϕ_e by specifying the axial density gradient, and the volume flux out of the estuary (V_{cc}) must be specified. For the Delaware Bay application, the subtidal outflow is

Table 1. Potential energy anomaly rate components for the unstratified and two-layer box models.

Variable	Name	Expression unstratified model	Expression two-layer model
Ω_1	potential energy influx from river	$P(g/2)(\rho_s - \rho_r)R$	$(g/4)(\rho_s - \rho_r)R$
Ω_2	outflux to coastal current	$-(g/2)(\rho_s - \rho_m)V_{cc}$	$-(g/4)(\rho_s - \rho_m)V_{cc}$
Ω_3	tidal mixing	–	$\frac{4\epsilon}{3\pi} C_d \rho_s u_t^3 A_e / h_e$
Ω_4	solar radiation	$\alpha g Q_s A_e / 2C_p$	$\alpha g Q_s A_e / 4C_p$
Ω_5	wind mixing	–	$\delta \kappa_s \rho_a \mid W \mid^3 A_e / h_e$
Ω_6	dense water inflow	–	$-(g/2)(\rho_s - \rho_L)V_L$

Table 2. Estuarine box model variables (after GW06).

Variable	Name
P	Factor set by profiles of current and ρ at river inflow
ρ_r	Density of river water (999.7 kg m^{-3})
R	River discharge (m^3 s^{-1})
ρ_m	Density at mouth of estuary (kg m^{-3})
V_{cc}	Volume flux of coastal current (m^3 s^{-1})
L_e	Distance from estuary mouth to fresh water (km)
X_e	Distance from estuary mouth to water of density ρ_e (km)
a	Surface area fraction covered by estuary box (m^2)
b	X_e/L_e parameter
ϵ	Mixing efficiency of tide (0.004)
C_d	Bottom drag coefficient
u_t	Root mean squared tidal current amplitude (m s^{-1})
u_{mod}	Tidal current amplitude modulation for neap-spring variations (m s^{-1})
h_e	Mean estuary depth (m)
α	Thermometric expansion coefficient (1.7×10^{-4}/K)
Q_s	Net solar radiation (Wm^{-2})
C_p	Specific heat of sea water (4200 J/kg^{-K})
δ	Mixing efficiency of wind constant (0.039)
k_s	Effective surface drag coefficient (6.4×10^{-5})
ρ_a	Air density at sea level (1.229 kg m^{-3})
W	Wind speed magnitude (m s^{-1})
W_x	Rotated wind component magnitude (m s^{-1})

computed empirically using a linear regression with low-passed wind and river discharge as independent variables:

$$V_{cc} = \overline{V}_{cc} + a_1(W_x - \overline{W}_x) + a_2(R - \overline{R}) \tag{4}$$

where the overbars indicate long term mean values, W_x is the wind component along the estuary axis (positive seaward), and R is river discharge lagged by 7 days. The linear regression coefficients are established in GW06 as $a_1 = 433$ m^{-2} and $a_2 = 2.54$. GW06 uses the climatological values $\overline{V}_{cc} = 8788$ m^3 s^{-1}, $\overline{W}_x = 0$ ms^{-1} and $\overline{R} = 577$ m^3 s^{-1}. Other box model inputs include time series of river discharge (for Ω_1 and V_{cc} in Ω_2), winds (for Ω_5 and V_{cc} in Ω_2), and surface heat flux (for Ω_4). The characteristic M_2 tidal current amplitude and spring-neap modulation force Ω_3. As explained below, the unstratified case cannot include tidal or wind mixing explicitly ($\Omega_3 = 0, \Omega_5 = 0$).

Volume conservation is used to find the time-varying landward flow through the mouth (V_L):

$$V_L = V_{cc} - R - V_Q. \tag{5}$$

Here V_Q reflects thermal expansion or contraction due to surface heat flux (Q); a typically small term neglected in GW06. Estuary water volume is considered constant. R and V_L are

positive into the estuary, V_Q is positive for heating, and V_{cc} is positive out of the estuary. Note that the landward Stokes transport (separately considered in GW06) is included here in V_L.

The box model conserves mass. In fact, the potential energy anomaly budget can be derived by combining volume and mass conservation. The form of the mass budget will be included for each case, but it is important to note that it does not introduce another independent equation. Figure 2 illustrates estuarine box model inputs, outputs and basic assumptions for the two box models.

c. *Unstratified model*

GW06 applied an unstratified box model to the Delaware Bay. This model is summarized to draw comparisons with the two-layer case and to correct errors in the original formulation. The most substantial error introduced the possibility of overmixing (i.e. more mixing than is realistic). Choosing an unstratified model implicitly assumes that tidal and wind mixing are always strong enough to mix away any stratification; this limiting case can be an appropriate choice for many estuaries (including the Delaware). In this case, the potential energy anomaly budget should not include vertical mixing terms since the water column cannot be further mixed. The correct ϕ budget is:

$$aA_e \frac{d\phi_e}{dt} = \Omega_1 + \Omega_2 + \Omega_4. \tag{6}$$

In GW06 Ω_3 and Ω_5 were included, but other factors minimized the error in the results. A computational error kept the calculated wind mixing (Ω_5) orders of magnitude too small. The tidal mixing (Ω_3) was largely offset by the nonzero annual mean heat flux (in Ω_4); the

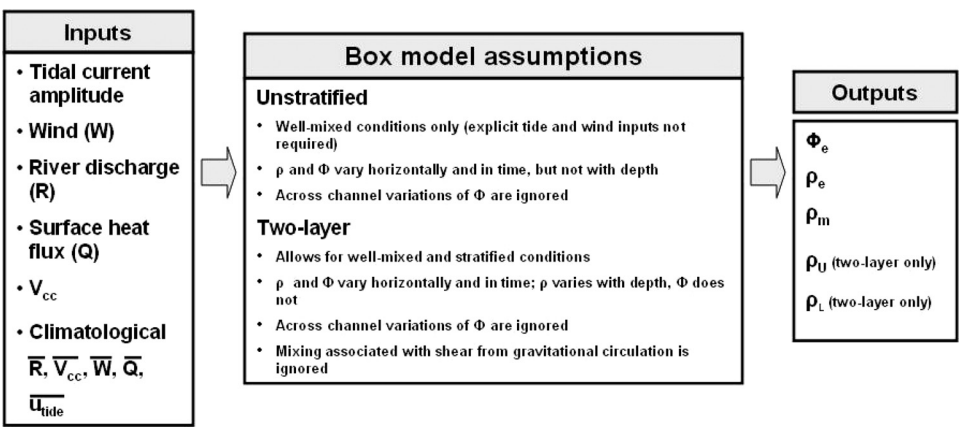

Figure 2. Diagram depicting the inputs, outputs and basic model assumptions of the unstratified and two-layer estuarine box models.

annual mean Q now is set correctly to zero to avoid long-term heating and cooling in the system.

The unstratified case divides the estuary laterally into two boxes: one side with low densities and seaward flow and the other side with the shelf reference density and landward flow. Since the landward water has a density of ρ_s, it carries no potential energy anomaly flowing into the estuary and thus $\Omega_6 = 0$. The box model is constructed for the active low-density side with volume aA_eh ($0 \leq a \leq 1$). GW06 implicitly set $a = 1$; $a = 0.2$ for the new computations to better reflect the Delaware regime. Corrected results for the GW06 study period are described in Section 3.

Conservation of mass for this box model is:

$$aA_eh\frac{d\rho_e}{dt} = \rho_r R + \rho_s V_L - \rho_m V_{cc}. \tag{7}$$

The river mass flux enters the estuary head, the buoyant outflow mass flux leaves through the mouth, and the landward dense-water mass flux enters along the box side that laterally divides the estuary. Note that surface heat flux has no mass flux directly associated with it, but the volume expansion and contraction ($V_Q = \alpha a A_e Q / C_p \rho_e$) does appear in the volume budget (5) used to calculate V_L.

The potential energy anomaly is area-averaged only over the seaward-flowing low-density box included in the model. ϕ changes associated with free surface height are small and are therefore ignored for simplicity. The ϕ_e is related to the average density ρ_e by integrating (2):

$$\phi_e = \frac{gh}{2}(\rho_s - \rho_e). \tag{8}$$

Similarly, the potential energy anomaly at the mouth of the estuary ϕ_m is defined as:

$$\phi_m = \frac{gh}{2}(\rho_s - \rho_m). \tag{9}$$

The box model specifies a linear density gradient increasing from ρ_r at distance L_e from the mouth to ρ_m at the mouth. At distance X_e from the mouth, the upper-estuary volume equals the lower-estuary volume and the local density equals the estuary-averaged density. The parameter $b = X_e/L_e$ is 0.5 for a constant-width constant-depth estuary; $b < 0.5$ for estuaries that widen and/or deepen toward the mouth. With the linear density gradient, ρ_e is related to ρ_m by:

$$\rho_e = (1 - b)\rho_m + b\rho_r. \tag{10}$$

By substituting the Ω terms (Table 1), the ϕ_e expression (8), and the axial density gradient (10) into the ϕ budget (6), a single equation for the unknown ρ_e is found:

$$\frac{d\rho_e}{dt} = -(\rho_s - \rho_r)\frac{R}{aA_eh} - \frac{\alpha\rho_s}{hC_p\rho_e}Q + \left[\rho_s - \frac{\rho_e - b\rho_r}{(1-b)}\right]\frac{V_{cc}}{aA_eh}. \tag{11}$$

Alternately, the above equation can be derived by substituting volume conservation (5) and the axial density gradient (10) into mass conservation (7). This equation can be numerically integrated with time-varying inputs of river inflow, surface heat flux, and empirically-derived coastal current volume flux. The resulting ρ_e time series can be used to calculate ϕ_e via (8) and ρ_m via (10). The model is initialized with the steady-state solution derived in Section 2e.

d. Two-layer model

Two-layer models allow for stratified and well-mixed conditions. The two-layer model developed here fixes the layer interface at half the total water depth ($d = h/2$) and allows the upper- and lower-layer densities to vary with time. The estuary-averaged potential energy anomaly budget for this case is:

$$A_e \frac{d\phi_e}{dt} = \Omega_1 + \Omega_2 + \Omega_3 + \Omega_4 + \Omega_5 + \Omega_6. \tag{12}$$

Note that tidal and wind mixing are explicitly included. The mixing terms are shut off when the water column becomes unstratified anywhere in the estuary; this threshold avoids overmixing and preserves the linear axial density gradient. The Ω_6 term arises because the lower layer contributes to ϕ_e changes when ρ_L becomes less than ρ_s after vertical mixing. The Ω expressions are listed in Table 1. The surface area fraction covered by the estuary box, a for this model is equal to 1.

Mass is conserved in the upper and lower layers (and the entire estuary):

$$\frac{A_e h}{2} \frac{d\rho_U}{dt} = \rho_r R + \rho_L V_L + -\rho_m V_{cc} + M_{mix} \tag{13a}$$

$$\frac{A_e h}{2} \frac{d\rho_L}{dt} = (\rho_s - \rho_L) V_L - M_{mix}. \tag{13b}$$

The upper-layer mass budget is similar to the unstratified case except for the additional mass flux associated with vertical mixing, $M_{mix} = (2/g)(\Omega_3 + \Omega_5)$. M_{mix} increases upper-layer density and decreases lower-layer density; $M_{mix} = 0$ when tidal and wind mixing are shut off. V_L can be calculated with the volume budget (5) and the expression for thermal expansion and contraction ($V_Q = \alpha A_e Q / C_p \rho_U$).

The estuary-averaged potential energy anomaly can be expressed in terms of the area-averaged upper and lower-layer densities (ρ_U and ρ_L, respectively) by integrating (2) for this situation:

$$\phi_{1_e} = \frac{gh}{8}(4\rho_s - 2\rho_L - 2\rho_U) \tag{14a}$$

$$\phi_{local_e} = -\frac{gh}{8}(\rho_L - \rho_U) \tag{14b}$$

$$\phi_e = \frac{gh}{8}(4\rho_s - 3\rho_L - \rho_U) \tag{14c}$$

where $\phi_e = \phi_{1_e} - \phi_{local_e}$. The potential energy anomaly at the mouth (ϕ_m) is defined as (here the lower layer density is always ρ_m):

$$\phi_{1_m} = \frac{gh}{8}(2\rho_s - 2\rho_m) \tag{15a}$$

$$\phi_{local_m} = -\frac{gh}{8}(\rho_s - \rho_m) \tag{15b}$$

$$\phi_m = \frac{gh}{8}(\rho_s - \rho_m). \tag{15c}$$

A linear density gradient is specified for the upper and lower layers. Upper layer density ranges from ρ_r at the head to ρ_m at the mouth. Lower layer density ranges from ρ_H (an additional unknown variable) at the head to ρ_s at the mouth. At X_e the local upper- and lower-layer densities equal ρ_U and ρ_L, respectively. With these linear gradients, ρ_U is related to ρ_m, ρ_L is related to ρ_H, and ρ_e is related to ρ_U and ρ_L by:

$$\rho_U = (1-b)\rho_m + b\rho_r \tag{16a}$$

$$\rho_L = (1-b)\rho_s + b\rho_H \tag{16b}$$

$$\rho_e = (\rho_U + \rho_L)/2. \tag{16c}$$

Note that (16b) is not necessary to complete the box model solution, but it can be used afterward to find ρ_H and the linear density distribution in the lower layer. Similarly, (16c) can be used to calculate the estuary-averaged density afterward.

For the two-layer case, it is most straightforward to numerically integrate a coupled set of equations for ρ_U and ρ_L derived by substituting volume conservation (5) and the upper-layer density gradient (16a) into the mass budgets:

$$\frac{d\rho_U}{dt} = -2(\rho_L - \rho_r)\frac{R}{A_e h} - \frac{2\alpha\rho_L}{hC_p\rho_U}Q + 2\left[\rho_L - \frac{\rho_U - b\rho_r}{(1-b)}\right]\frac{V_{cc}}{A_e h} + \frac{4(\Omega_3 + \Omega_5)}{gA_e h} \tag{17a}$$

$$\frac{d\rho_L}{dt} = \frac{2(\rho_s - \rho_L)}{A_e h}\left[-R - \frac{\alpha A_e}{C_p\rho_U}Q + V_{cc}\right] - \frac{4(\Omega_3 + \Omega_5)}{gA_e h}. \tag{17b}$$

These equations can be substituted into the time derivative of (14c) to give the left-hand side of (12) and yield the ϕ_e budget.

The coupled equations (16) can be numerically integrated with forcing from river inflow, surface heat flux, winds, tidal current amplitudes, and the empirically derived coastal current volume flux. The resulting ρ_U and ρ_L can be used to calculate ρ_m, ρ_H, and ρ_e via (15c). The model is initialized with the steady-state solution derived in Section 2e.

e. Steady-state solutions

The steady-state solution for the unstratified case is found by setting the left-hand side of (11) to zero, setting variables to mean values and solving for ρ_e:

$$\overline{\rho_e} = \rho_r + (1-b)\left[(\rho_s - \rho_r)\left(1 - \frac{\overline{R}}{\overline{V}_{cc}}\right) - \frac{aA_e\alpha\overline{Q}}{C_p\overline{V}_{cc}}\right]. \tag{18}$$

The density ratio in the $\overline{Q}$ term is set to one for simplicity. The steady-state $\overline{\phi_e}$ is then found by substituting ρ_e into (8).

For the two-layer case, the steady-state solution is derived by setting the left-hand side of (17a) and (17b) to zero, setting variables to mean values and solving for $\overline{\rho_L}$ and $\overline{\rho_U}$. Note that the density ratio in the Q term is set to one in (17a) and $\overline{\rho_U}$ is approximated as ρ_s in the Q term in (17b). The variable $\overline{\rho_L}$ is solved for first, then $\overline{\rho_U}$ can be found. Wind mixing is set to zero for the mean state. Note that if tidal mixing is set to zero, $\overline{\rho_L} = \rho_s$ and $\overline{\rho_U}$ is almost exactly $\overline{\rho_e}$ from the unstratified case:

$$\overline{\rho_L} = \rho_s - \frac{2\overline{\Omega_3}}{g}\left[-\overline{R} - \frac{\alpha A_e}{C_p\rho_s}\overline{Q} + \overline{V}_{cc}\right]^{-1} \tag{19}$$

$$\overline{\rho_U} = \rho_r + (1-b)\left[(\rho_L - \rho_r)\left(1 - \frac{\overline{R}}{\overline{V}_{cc}}\right) - \frac{A_e\alpha\overline{Q}}{C_p\overline{V}_{cc}} + \frac{2\overline{\Omega_3}}{g\overline{V}_{cc}}\right]. \tag{20}$$

The steady-state $\overline{\phi_e}$ is then found by substituting (19) and (20) into (14c).

3. Box model application to Delaware Bay for the GW06 study period

a. Model initialization

We applied the unstratified and two-layer potential energy estuarine box models to the Delaware Bay for the GW06 1988 to 1994 model period using a time step of 1 day. Following GW06, we adjusted the maximum heat flux to coincide with the time of the summer solstice and initialized the models by setting climatological value of wind ($\overline{W}_x$) to zero, volume flux ($\overline{V}_{cc}$) to 8788 $m^3\ s^{-1}$ and river discharge ($\overline{R}$) to 577 $m^2\ s^{-1}$ (i.e. the computed mean discharge for the period 1988-1994). In addition we set the climatological value of heat flux ($\overline{Q_s}$) to zero. The initial density and ϕ_e values were set to climatological values computed as described in the last section. For the unstratified model $\overline{\rho_e} = 1016\ kg\,m^{-3}$ and $\overline{\phi_e} = 352\ J\,m^{-3}$. For the two-layer model $\overline{\rho_L} = 1019\ kg\,m^{-3}$, $\overline{\rho_U} = 1016\ kg\,m^{-3}$, and $\overline{\phi_e} = 239\ J\,m^{-3}$. We set the climatological value for the tide ($\overline{u_{tide}}$) to the RMS tidal current amplitude of 0.5 ms^{-1}. For the two models we set the seasonal heat flux amplitude ($Q_{seasonal}$) to 89 Wm^2 and in the unstratified model $P = 1$, as in GW06. The latter represented a river inflow with no vertical shear. We used a $\rho_s = 1025\ kg\,m^{-3}$ and $\rho_r = 999.5\ kg\,m^{-3}$. For the Delaware Bay, $h_e = 8$ m, $A_e = 2.1 \times 10^9\ m^2$, $X_e = 30$ km, $L_e = 97$ km, and $b = 0.3$. Other model variables used for Delaware Bay are summarized in Table 3.

Table 3. Estuarine box model variables used for Delaware Bay in the unstratified and two-layer model versions.

Variable	Value
a_1	433
a_2	2.54
C_d	0.0025
u_t	0.6 m s^{-1}
u_{mod}	0.1 m s^{-1}
A_e	2.1×10^9 m^2
X_e	30×10^3 m^3
L_e	97×10^3 m^3
a	0.2
b	0.3
P	1
h_e	8 m
ρ_s	1025 kg m^{-3}
Q_s	0 Wm^{-2}; seasonal flux = 89 Wm^{-2}
$\overline{V_{cc}}$	8788 m s^{-3}
$\overline{W_x}$	0 m s^{-2}
$\overline{u_t}$	0.6 m s^{-1}
$\overline{R}$	577 m^3 s^{-1}
$\overline{Q_s}$	0 W m^{-2}

Following GW06 we used the component of the hourly Atlantic City winds aligned with 135°T to characterize along-estuary winds. To estimate the riverine freshwater inflow (R), the hourly Trenton River discharge was used; discharge values were divided by 0.58 to account for other sources of freshwater into the bay (Whitney, 2006).

b. Unstratified box model results

Figure 3 is a corrected version of Figure 4 in the GW06 paper. It shows ϕ_e variation rates and levels of Ω_i for the year 1993. Even in the absence of explicit tidal and wind effects, the new unstratified model results are generally similar to results in GW06. As discussed, this is primarily due to the computational error in the wind term, which kept the term orders of magnitude too small, and to the use of a nonzero annual mean heat flux, which largely offset the tidal (Ω_3) term. The main difference is observed in the $d\phi/dt$ curve, which no longer exhibits tidal modulation effects. As found in GW06, the largest contributor of potential energy to the estuary is the river discharge, primarily due to the two high discharge events in the months of April and December. With a mean magnitude of $\overline{\Omega_1} = 7.2 \times 10^5$ J m^{-1} s^{-1}, the river discharge term is closely followed (but with opposite sign) by the coastal current efflux term ($\overline{\Omega_2} = 7.1 \times 10^5$ J m^{-1} s^{-1}). This term contributes to the depletion of potential energy in the estuary. In comparison to the Ω_1 and Ω_2

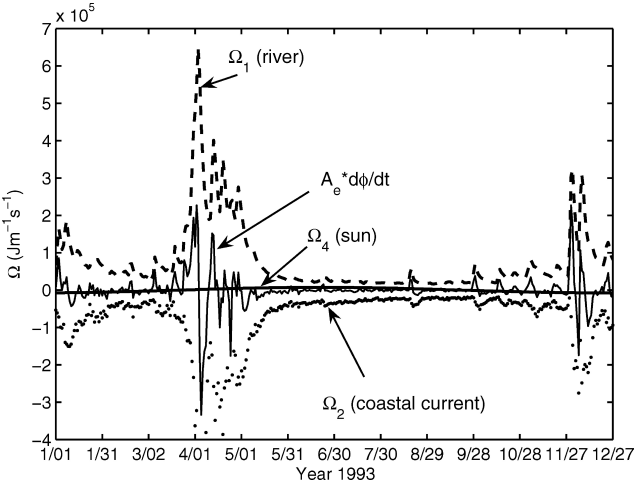

Figure 3. Corrected GWO6 time series of Delaware Bay rates of change of potential energy anomaly for the year 1993 obtained from the unstratified box model. The competing mechanisms for the unstratified model are the river (Ω_1), coastal current (Ω_2) and solar heat (Ω_4).

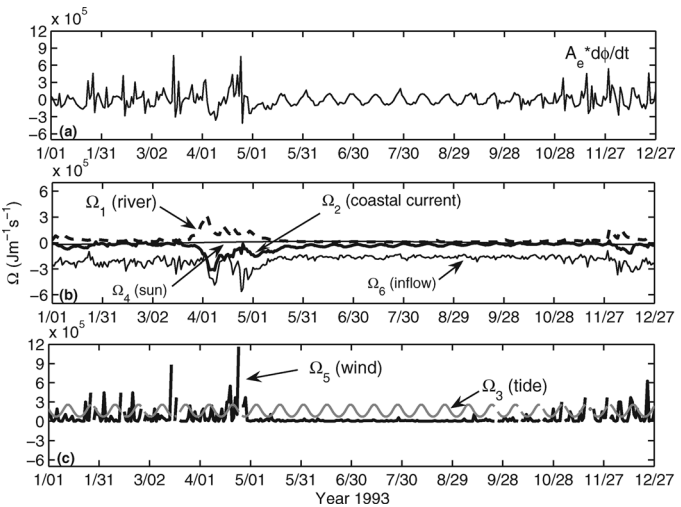

Figure 4. Time series of the rates of change of potential energy anomaly for Delaware Bay in 1993 obtained from the two-layer box model. In addition to the river, coastal current and solar heat mechanisms, the two-layer model also incorporates tidal (Ω_3), wind (Ω_5) and dense inflow (Ω_6) mechanisms. The $A_e * d\phi/dt$ term is shown in panel (a), river, coastal current, solar and dense inflow terms in panel (b), and the tidal and wind terms in (c). For clarification purposes panel (b) is plotted on a different scale than panels (a) and (c).

terms, solar heating ($\overline{\Omega_4} = 7.8\ \mathrm{J\,m^{-1}\ s^{-1}}$) makes only a small contribution to the potential energy. Tidal and wind mixing are implicitly considered always strong enough to counter stratifying influences of river inflow and surface heating and keep the estuary vertically well mixed.

c. Two-layer box model results

Figure 4 shows variations and rate levels of Ω_i from the two-layer model for the year 1993. For clarification purposes panel (b) is plotted on a different scale than panels (a) and (c). In contrast to the unstratified model results, the coastal current efflux and $d\phi/dt$ curves now co-vary with wind events. In addition, the effect of the neap-spring tidal variability is now clearly evident in the two curves during the summer months, where strong wind events are absent. This variability is not present in the unstratified results due to constant mixing levels set in the model.

The largest contributor in the two-layer case, with a mean magnitude of $\overline{\Omega_6} = -2.9 \times 10^5\ \mathrm{J\,m^{-1}\ s^{-1}}$, is the dense inflow term. On average this term balances out the tide and wind-mixing terms, which tend to increase the potential energy in the system. Since it has a negative sign, the dense inflow term acts to lower ϕ. The wind term is the second largest contributor ($\overline{\Omega_5} = 1.7 \times 10^5\ \mathrm{J\,m^{-1}\ s^{-1}}$), followed by the tide ($\overline{\Omega_3} = 1.6 \times 10^5\ \mathrm{J\,m^{-1}\ s^{-1}}$), river discharge ($\overline{\Omega_1} = 5.6 \times 10^4\ \mathrm{J\,m^{-1}\ s^{-1}}$), coastal current efflux ($\overline{\Omega_2} = -4.8 \times 10^4\ \mathrm{J\,m^{-1}\ s^{-1}}$) and lastly the surface heat flux term ($\overline{\Omega_4} = 3.9 \times 10^3\ \mathrm{J\,m^{-1}\ s^{-1}}$).

Contrary to the remarks made in GW06, the wind term is a large contributor to the system (i.e. the largest peak registers at $11 \times 10^5\ \mathrm{J\,m^{-1}\ s^{-1}}$) and, except during the summer months, wind mixing is intermittently important. The two large peaks in river discharge observed in the unstratified layer results (Fig. 3) in the months of April and December and the corresponding coastal current efflux peaks from the discharge, are also detected in the two-layer model results, although the magnitude of the events are dampened by about half. The lower variability reflects competing responses to high river discharge; the stratification increase due to increased river inflow partially counters the depth average density and buffers ϕ_e changes.

Results of ϕ_e for 1993 from the unstratified and two-layer models can be compared in Figure 5. The two models exhibit some similar ϕ_e variability, with the signature of the two freshwater events of April and December apparent in both the time series. On average, the ϕ_e results for the unstratified model are about 35% larger than the two-layer ϕ_e. Analysis of Eq. (2) answers the discrepancy. In the unstratified case we have assumed a locally well-mixed water column, so that $-\phi_{local}$ (second term in Eq. 2) is always zero and ϕ_e is controlled entirely by ϕ_1. In contrast, the two-layer case usually is stratified. This stratification creates a $-\phi_{local}$ that competes with ϕ_1 and lowers the ϕ_e values. The two models are plausible for the Delaware Bay and there exists an uncertainty as to which one is more correct. A discussion of model performance is presented in Section 4c.

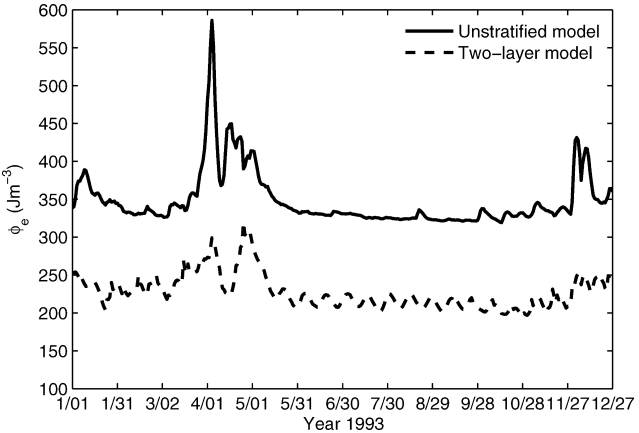

Figure 5. Comparison of Delaware Bay box model results of ϕ_e for the unstratified and two-layer models for the year 1993.

4. Box model application for Delaware Bay in Spring 2003

We applied the unstratified and two-layer potential energy estuarine box models to the Delaware Bay for the period January 1 to May 10, 2003 using a time step of one hour. Even though the available observations at mooring DC were for the period April 10 to May 10, we began the model runs three months ahead of the observations in order to allow sufficient time for adjustments to initial conditions to take place. Model variables, including initialization variables, were identical to the previous runs.

a. Box model results

Figure 6 shows the time series of the ϕ_e rate of change variations and Ω_i from the unstratified model from March 1 to May 10, 2003. The magnitude hierarchy of the average Ω terms is identical to the GW06 case. River discharge is initially low (Ω_1 values are about 0.8×10^5 J m^{-1} s^{-1}) until March 17, where a large discharge event (with maximum Ω_1 values reaching 5×10^5 J m^{-1} s^{-1}) causes rapid increase of potential energy in the estuary. Subsequent small discharge events occur on March 30, April 14 and May 5; however, the Ω_1 term has a decreasing trend to the end of the study period. The rapid increase in potential energy from the large discharge event is compensated by the coastal current efflux term, which acts to deplete ϕ in the system. This compensation occurs during a two to three week period and is clearly observed in the strong variability of the $d\phi/dt$ term. Except for the latter periods, $d\phi/dt$ is stable throughout the time series. The solar term (Ω_4), through its heating effect, contributes to the availability of potential energy, but it is the smallest contributor in the system.

Figure 7 shows time series of the ϕ_e rate of change and Ω_i from the six different competing mechanisms for the two-layer Spring 2003 model run. For clarification purposes panel (b) is

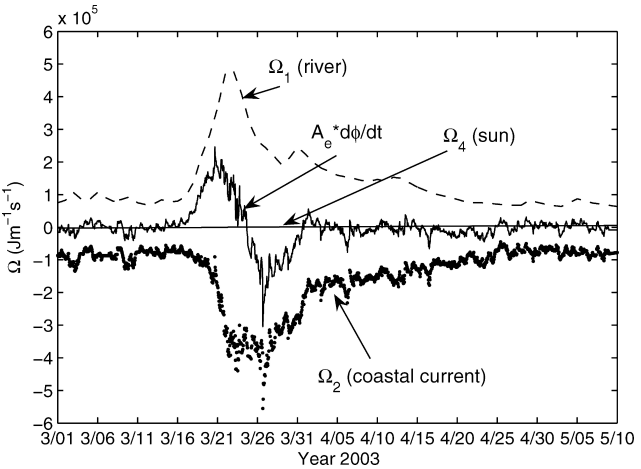

Figure 6. Time series of the rates of change of potential energy anomaly for the three competing mechanisms for Delaware Bay from March 1 to May 10, 2003 for the unstratified model.

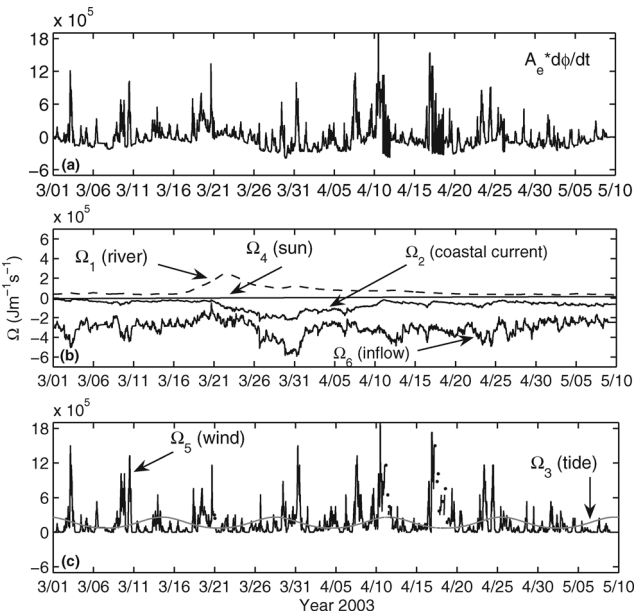

Figure 7. Time series of the rates of change of potential energy anomaly for the six competing mechanisms for Delaware Bay from March 1 to May 10, 2003 for the two-layer model. The $A_e * d\phi/dt$ term is shown in panel (a), river, coastal current, solar and dense inflow terms in panel (b), and the tidal and wind terms in (c). for clarification purposes panel (b) is plotted on a different scale than panels (a) and (c).

plotted on a different scale than panels (a) and (c). In accordance with the GW06 two-layer model results, the largest contributor is the dense inflow term (Ω_6), followed by the wind (Ω_5), tide (Ω_3), river discharge (Ω_1), coastal current efflux (Ω_2) and lastly the surface heat flux term (Ω_4). The 14-day tidal variability and wind variability are detected in the $d\phi/dt$ curve; however, the neap-spring tidal variability is not detected in the costal current efflux term due to the presence of strong wind events throughout the study period. The influence of seven strong wind events (with peaks larger or equal to 11×10^5 J m^{-1} s^{-1}) are evident in Figure 7. The same events can also be observed in Figure 8, which is the wind record for Atlantic City for the model period March 1 to May 10, 2003. The events have magnitudes ranging from 8–10 ms^{-1}; there are four upwelling favorable and three downwelling favorable events. The strong upwelling events occur on March 2-4, March 8-11, March 30-April 1 and April 23-25, while the downwelling events on March 17-20, April 7-12, and April 17-21. Note that even with the high occurrence of strong winds in the study period, the coastal current efflux term is generally more responsive to river discharge than wind effects.

Unstratified and two-layer box model results of the ϕ_e and ϕ_m are shown in Figure 9 (a) and (b), respectively. The thin vertical lines in the figure represent the seven strong wind events identified in Figures 7 and 8 at the time of maximum wind speeds. Results of ϕ_e and ϕ_m for the unstratified model have mean values of 360 J m^{-1} and 75 J m^{-1}, respectively, and appear to be stable over the model period, except for the large ϕ_e and ϕ_m peaks near March 25. This potential energy anomaly peak is driven by the imbalance of the river discharge and the coastal current efflux Ω terms as a result of the large river discharge event depicted in Figures 6 and 7(a). On average, potential energy anomaly ϕ_e and ϕ_m results for the two-layer model are about 25% and 60% smaller, respectively, than for the unstratified results ($\overline{\phi_e} = 300$ J m^{-3}, $\overline{\phi_m} = 27$ J m^{-3}). On monthly time scales ϕ results for this model are less variable than the unstratified results. This is due to the smaller ϕ_e and ϕ_m magnitudes, smaller peaks related to river discharge, and the balancing effects of ϕ produced by the dense inflow term (Ω_6). On daily to weekly time scales, variability

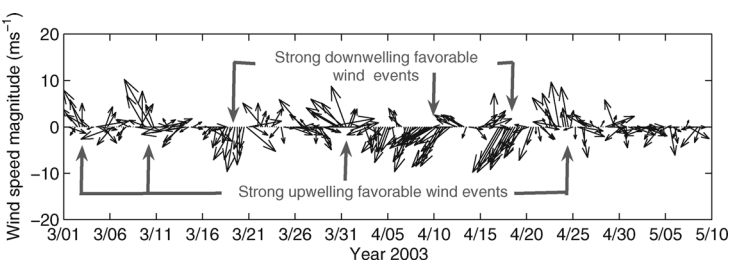

Figure 8. Wind record from Atlantic City from March 1 to May 10, 2003. Note the strong (8–10 ms^{-1}) downwelling-favorable wind events on March 17-20, April 7-12, and April 17-21, and the strong upwelling events on March 2-4, March 8-11, March 30-April 1 and April 23-25.

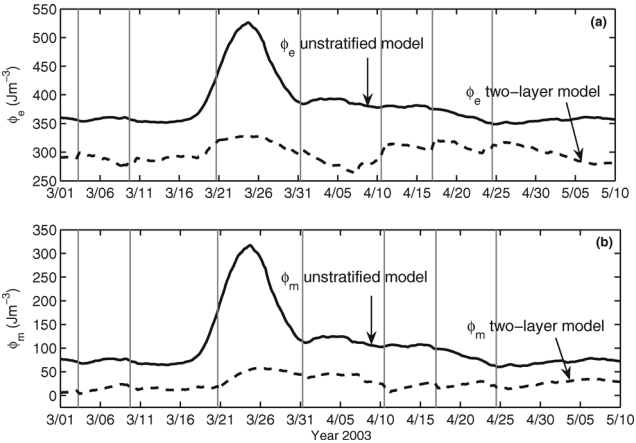

Figure 9. Comparison of Delaware Bay unstratified and two-layer box model results of ϕ_e(a) and ϕ_m (b) from March 1 to May 10, 2003. The thin vertical lines depict the times of maximum wind speed of seven strong (8-10 m s^{-1}) upwelling- and downwelling-favorable wind events.

associated with strong wind events (magnitudes larger or equal to 8 ms^{-1}) can be detected in the two-layer model results of ϕ. During these wind events the estuary average potential energy anomaly increases, while at the mouth the anomaly decreases. These responses are best explained with the aid of Eqs. (14a,bc) and (15a,b,c). Wind mixing increases the estuary average upper-layer density and decreases the lower-layer density by the same magnitude. This response leaves the depth-average density, and thus ϕ_{1_e}, unchanged and causes the ϕ_{local_e} term to become less negative; this results in increased ϕ_e. At the mouth, wind mixing increases the upper-layer density (ρ_m), but the lower-layer density remains fixed at ρ_s due to the landward flow of shelf water. This response decreases ϕ_{1_m} by increasing the depth-average density and causes the -ϕ_{local_m} term to become less negative; ϕ_m decreases because the change in ϕ_{1_m} is always twice the -ϕ_{local_m} change.

Figure 10 shows the time series of estuarine averaged density (ρ_e) for the unstratified and two-layer models and the upper and lower layer density (ρ_U and ρ_L) series for the two-layer model. The differences in ρ_e between the two model results are 1 to 2 kg m^{-3}; except during the large river discharge event in March, where density differences reach 4 kg m^{-3}. It is important to point out that the unstratified model ρ_e time series is by definition fresher than the two-layer model series. This is due to the fact that the density is computed only in the low-density outflowing side in the unstratified model. In contrast, the two-layer model ρ_e is the average density in the upper and lower layers and includes the entire estuary. The ρ_e in the unstratified model and the ρ_U in the two-layer model track each other well ($r = 0.7$) because the river inputs (R) and the mouth outflow (V_{cc}) are the same in both cases. Differences between the two curves are generally related to the lack of explicit wind mixing in the unstratified ρ_e curve.

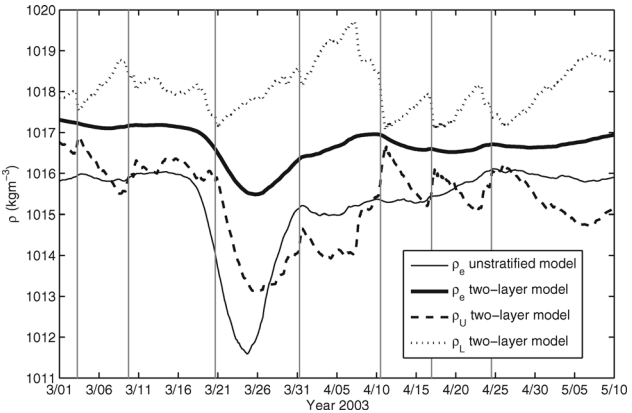

Figure 10. Results of Delaware Bay ρ_e, ρ_U and ρ_L from the two-layer model and ρ_e from the unstratified model for the period March 1 to May 10, 2003. The thin vertical lines depict the times of maximum wind speed of seven strong (8-10 m s^{-1}) upwelling- and downwelling-favorable wind events.

The effects of stratification and mixing in the two-layer model can be identified by the symmetry of the ρ_U and ρ_L curves. The separation of the curves during the high river discharge event in late March and between the strong wind events is indicative of stratification in the water column, while the de-stratification of the water column due to vertical mixing is visible during the wind events. Mean values of $\overline{\rho_U}$ and $\overline{\rho_L}$ are 1015.3 and 1018.1 kg m^{-3}, respectively. The high levels of R during the river discharge event causes a freshening of the estuarine upper-layer density, which in turn causes the estuarine depth-averaged density $\overline{\rho_e}$ to decrease. The resulting coastal current outflow (through V_{cc}) produces an increased V_L inflow that increases the lower-layer density. This eventually causes the estuarine-averaged density to increase back to background levels of about 1017.5 kg m^{-3}. During strong wind events, the upper-layer densities are increased due to mixing with lower-layer densities. However, as discussed, since vertical mixing associated to wind cannot directly change the estuarine average density, the lower-layer waters become fresher to offset the increase in density in the upper layer. Results of density time series at the mouth for the two models are discussed in Section 4c.

b. Potential energy computation from observations at mooring DC

Low pass filtered density data from mooring DC were used to compute the potential energy anomaly at the mooring site. In order to compare model results to observations, density data at the mooring were extrapolated to hourly from 15 minute samples. Data were also interpolated to 1 m intervals in the vertical. The depth-averaged potential energy ϕ_{DC} was computed from (2), using a depth $h_{DC} = 18$ m. As in the box models, we used a ρ_s of

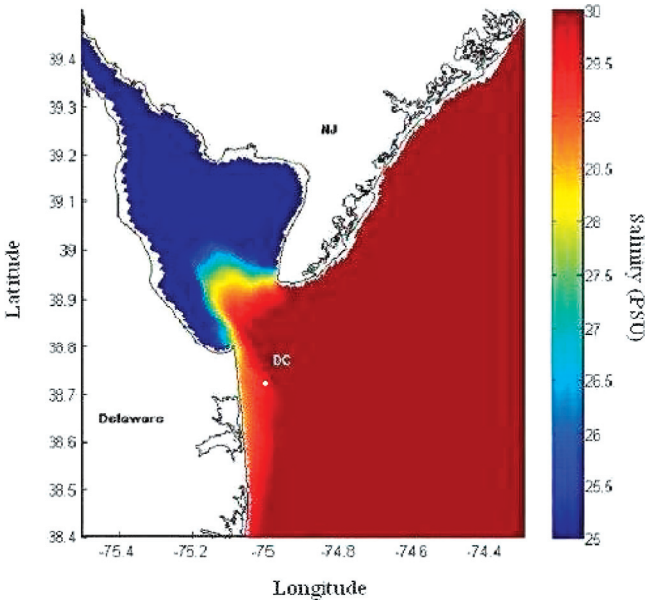

Figure 11. Results of depth-averaged salinity of the Delaware Bay region obtained from an ECOM 3D model run averaged over the observation period April 10 to May 10, 2003.

1025 kg m^{-3}. The depth-averaged density time series from the mooring is used to compare to the model time series.

Figure 11 shows results from an ECOM3D model run of depth-averaged salinity in the Delaware Bay region averaged over the observational time period of April 10 to May 10, 2003. While the average salinity across the estuary mouth is about 28.5 PSU, the average salinity at mooring DC is of the order of 29.5 PSU. Due to this 1 PSU salinity difference we anticipate the observed densities will be higher than model results for the mouth. The proximity of the mooring to the mouth makes comparisons with model results a worthwhile endeavor. It should be noted that the mooring site is influenced by both estuarine and shelf processes so perfect agreement is not expected.

c. Comparison of potential energy box model results to observations

Figure 12 shows the observed and modeled time series of potential energy anomaly at the estuary mouth (ϕ_m) and Figure 13 shows time series of mouth density ρ_m. In order to detect stratified and mixed regimes at the mooring site, density contours at 1, 6, 12 and 18 m depth are also displayed on the latter figure. The model ϕ_m was computed by solving (9) for the unstratified case and (15c) for the two-layer case. At the beginning of the time series (April 10) the observed level of potential energy anomaly at the mouth is 100 J m^{-3}. The reason for the initial increase of ϕ_m to 150 J m^{-3} is unclear since it occurs during

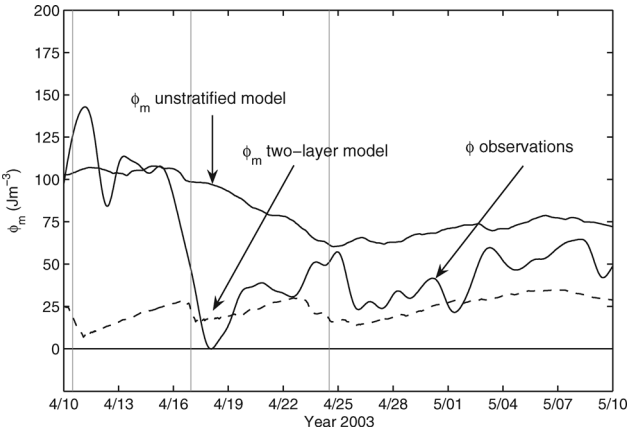

Figure 12. Comparison of Delaware Bay results of ϕ_m from the unstratified and two-layer models and observations for the period April 10 to May 10, 2003. The thin vertical lines depict the times of maximum wind speed of seven strong (8-10 m s^{-1}) upwelling and downwelling-favorable wind events.

a strong downwelling favorable wind event; however, since the observation time series starts halfway through the event, we do not speculate further on this matter. The complete depletion of ϕ_m observed near April 18 is linked to the strong downwelling-favorable wind

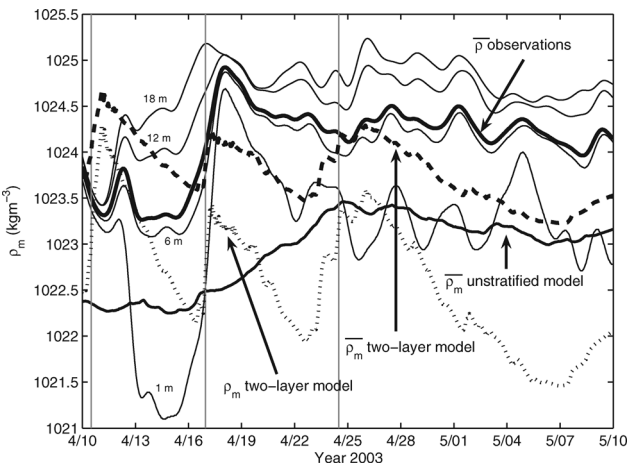

Figure 13. Comparison of Delaware Bay results of $\overline{\rho_m}$ for the unstratified and two-layer models, upper layer density (ρ_m) for the two-layer model and $\overline{\rho}$ for the observations from April 10 to May 10, 2003. In order to detect stratified and mixed regimes at the mooring site, density contours at 1, 6, 12 and 18-m depth are also displayed on the figure. The thin vertical lines depict the times of maximum wind speed of seven strong (8-10 m s^{-1}) upwelling- and downwelling-favorable wind events.

event that occurs on April 17-21. It is important to note that since mooring DC is located on the shelf, the decrease in stratification during the downwelling event is not likely due only to vertical wind mixing, but also from isopycnal tilting (or straining) associated with the cross-shelf Ekman transport (e.g. Fong and Geyer, 2001; Whitney and Garvine, 2005). The response of potential energy anomaly during the strong upwelling wind event on April 23-25 differs from the downwelling response. During this event the depth-averaged density at the mooring experiences a general but small decrease, which in turn produces a general but small (about 20 J m^{-3}) increase in ϕ_m. The small response in the depth-average density and potential energy anomaly, in addition to the lack of mixing observed during the event, makes the role of this strong upwelling wind event unclear. We speculate that any vertical mixing that takes place during the event may perhaps be inhibited by the stratification effects from offshore Ekman transport.

The unstratified model trends of ϕ_m track some of the observed trends. Initial model values of 100 J m^{-3} agree with initial mooring values, and similarly to the observations ϕ_m experiences a general decrease from the beginning of the series to April 25, and then an increase from April 25 to the end of the time series. The model results, however, exhibit less variability and are on average larger than the observed ϕ by 25 J m^{-3}. The assumption of a well-mixed water column, which as discussed increases potential energy anomaly values and eliminates the response to individual wind events, partly explains the mismatch and lack of model variability. The approximate 1 PSU salinity difference between the estuary mouth and the location of mooring DC, which in turn causes lower model ρ_m values by on average 1-1.5 kg m^{-3} (Fig. 13), also contributes to the larger values of potential energy anomaly in the model.

In contrast to the unstratified model results of ϕ, the two-layer model results on average underestimate the observations by about 30 J m^{-3}. This result causes the observed potential energy anomaly curve to be bracketed between the two model results. It is unclear why the two-layer model ϕ_m values are much lower compared to the observations at the beginning of the series, however after the passing of the second downwelling wind event on April 18 the two-layer model results qualitatively track the observations well. In contrast to the unstratified model results, variability in potential energy anomaly due to the wind events is detected in the two-layer model ϕ_m results; however, the ϕ_m variability is lower than the observed ϕ variability. As discussed in Figure 9(b), ϕ_m values decrease during the events while ρ_m values (Fig. 13) increase. We note that care must be taken when comparing ρ_m time series for the two-layer model with the $\overline{\rho}$ from the observations and $\overline{\rho_m}$ from the unstratified model. The latter two densities are depth-averaged, while ρ_m for the two-layer model represents the density in the upper layer. A better match of the two-layer ρ_m series is, for example, the 1-m density contour from the DC mooring. We can, however, compute the two-layer depth-averaged density at the mouth as: $\overline{\rho_m} = (\rho_m + \rho_s)/2$ and compare it to the observed $\overline{\rho}$ (see Fig. 13). Similarly to the unstratified model results, comparisons between the $\overline{\rho_m}$ curve for the two-layer model and the observed $\overline{\rho}$, and the

two-layer ρ_m curve and the observed 1-m curve, reveal on average a 1 kg m^{-3} (plus or minus in this case) density difference. At the mouth, the average density in the upper layer of the two-layer model (ρ_m) is 1022.6 kg m^{-3}, while in the lower layer it is 1025 kg m^{-3} (or ρ_s).

To quantitatively compare ϕ_m model results to the observations, we adopted the statistical method of Oke *et al.* (2002). We computed the correlation coefficient, (r), model bias (MB), defined as the difference between the mean model value and the mean observed value, the standard deviation error (STDE), or difference between the standard deviation of the model results and the observed standard deviation, and the root mean square error (RMSE). Table 4 shows the results from the statistical computations. The correlation coefficients for both models are statistically insignificant. Even though the unstratified model r is relatively high (i.e. 0.68), the time series has only five effective degrees of freedom. Consequently the 95% significant r value (in brackets in Table 4) is 0.96. The two-layer model series has 10 effective degrees of freedom and a 95% significant r value of 0.66. For the unstratified model, the MB value is 26.8 J m^{-3}, indicating that the model is on average overestimating the potential energy anomaly by 67%. The two-layer model MB values is on the other hand -30.9 J m^{-3}, which is indicative the model is underestimating the observations by 57%. The STDE for the unstratified model is negative and large (-16.9 J m^{-3}), which is an indication that the model is able to capture only about 5% of the observed variability in the system. In the two-layer model the value of STDE is larger (-25.7 J m^{-3}) indicating that the model is able to capture only 2% of the observed variability. The RMSE value, which attests to the overall performance of the models, is 36.9 J m^{-3} for the unstratified model and 46.3 J m^{-3} for the two-layer model. The latter values translates to an overall 27% and 31% model error, respectively. Despite the statistically insignificant correlations, the overall analysis suggests the unstratified model results are statistically better than the two-layer model results for the observation period. The results of MB, STDE and RMSE from the quantitative analysis however improve considerably for the two layer model if the statistics are computed from April 18 to the end of the time series. In this case the values of MB, STDE and RMSE decrease to -14.7 J m^{-3}, -8.18 J m^{-3} and 18.8 J m^{-3}, respectively.

Table 4. Statistics computed for ϕ_m results between observations at mooring DC and the box models. r is the correlation coefficient. The 95% significant r values are shown in brackets. MB stands for model bias, $STDE$ standard deviation error, and $RMSE$ root mean square error. After Oke *et al.* (2002).

Variable	Value unstratified model	Value two-layer model	Value two-layer model after April 18
r	0.68 (0.96)	-0.21 (0.66)	0.60 (0.75)
MB	26.8 J m^{-3}	-30.9 J m^{-3}	-14.7 J m^{-3}
$STDE$	-16.9 J m^{-3}	-25.7 J m^{-3}	-8.18 J m^{-3}
$RMSE$	36.9 J m^{-3}	46.3 J m^{-3}	18.8 J m^{-3}

5. Summary and conclusions

We have corrected an unstratified estuarine box model of potential energy anomaly, initially developed by Garvine and Whitney (2006), and have developed a two-layer estuarine box model that allows for stratification and mixing conditions. Both models have been used as low level interpretive tools to assess the mixing dynamics in the Delaware Bay. Unstratified model results for the two study periods reveal that the river discharge (Ω_1) is the largest potential energy anomaly contributor. This term is closely followed (but with opposite sign) by the coastal current efflux term (Ω_2). For the two-layer model the largest contributor is the dense inflow term (Ω_6). The wind (Ω_5) is the second largest term in the two-layer model, followed by the tide (Ω_3), river discharge (Ω_1) and coastal current terms. In both models the solar heat flux term (Ω_4) makes the smallest contribution to ϕ.

Spring 2003 model results have been compared to observations located on the Delaware shelf. Correlation coefficients between observations and the models are statistically insignificant for the one-month comparison; however, other statistics such as the RMSE indicate that the unstratified model overall performs better than the two-layer model for the period and so it is selected on this basis. If the interest is on the importance of tides and winds to the potential energy anomaly in the system, or on the response of ϕ during strong wind events, the two-layer model is however preferable. While there is no clear model choice for the Delaware Bay, it is important to note that for highly stratified estuaries the unstratified model may be entirely inappropriate. Therefore, for these estuaries the two-layer model would have to be selected.

Both the qualitative and quantitative analyses presented convey some agreement and disagreement between the model results and the observations. The model limitations associated with simplification of the dynamical processes undoubtedly play a large role in the observed discrepancies; however, as discussed, it is also likely that natural differences between conditions at the mouth and the instrument location on the nearby shelf contribute to model-observation mismatch. Processes such as isopycnal tilting and offshore Ekman transport, which may contribute to the variability of ϕ depicted in the observations, are strictly shelf processes and are therefore not included in the model dynamics. It is also important to note that the general 1–1.5 kg m^{-3} density disagreement between model and observed results, which is consistent with the approximate 1 PSU salinity increase from the mouth to the location of mooring DC, is of the order of the typical average density anomaly of the Delaware Coastal Current originating from the bay (Münchow and Garvine, 1993 a,b). This implies that comparing results at the mouth with observations on the shelf always produces an error that is of the scale of the feature that is being modeled.

In conclusion, we speculate that model comparisons to density observations at the mouth (perhaps obtained from transects at the mouth from an undulating CTD) would result in better agreement, and therefore we encourage such a task in the near future. The availability of high-resolution density data at the mouth would also allow the box model outflowing density variable ρ_m to be known and therefore would permit the variable V_{cc} to be a model

unknown. Furthermore, the availability of this type of data would particularly be helpful for the application of the box models to other estuaries, where the empirical V_{cc} relation (4) is not applicable and an empirical relation of V_{cc} is unknown.

Acknowledgments. We would like to thank A. D. Kirwan, Jr. and Felipe Pimenta for providing valuable discussions and useful comments in the writing process of the manuscript. We are indebted to two anonymous reviewers for helping us find a fundamental error in the box model methodology. We would also like to thank Alan Blumberg for access to the model ECOM3D. This work was supported by the National Science Foundation through grant OCE-0220446 to the University of Delaware. We are grateful to have known Rich and we are honored to have had the opportunity to work with him through the years.

REFERENCES

Austin, J. A. 2002. Estimating the mean ocean-bay exchange rate of the Chesapeake Bay. J. Geophys. Res., *107*, C11, 3192, doi 10.1029/2001JC001246.

Fong, D. A. and W. R. Geyer. 2001. Response of a river plume during an upwelling favorable wind event. J. Geophys. Res., *106*, 1067-1084.

Garvine, R. W. 1995. A dynamical system for classifying buoyant coastal discharges. Cont. Shelf Res., *15*, 1585–1596.

Garvine, R. W. and M. M. Whitney. 2006. An estuarine box model of freshwater delivery to the coastal ocean for use in climate models. J. Mar. Res., *64*, 173–194.

Hamilton, P., J. T. Gunn and G. A. Cannon. 1985. A box model of Puget Sound. Estuar. Coast. Shelf Sci., *20*, 673–692.

Henrichs, S., N. Bond, R. W. Garvine, G. Kinecke and S. Lohrenz. 2000. Coastal Ocean Processes (CoOP): Transport and transformation processes over continental shelves with substantial freshwater inflows. CoOP report number 7.

Longuet-Higgins, M. S. 1969. On the transport of mass by time-varying ocean currents. Deep-Sea Res., *116*, 431–447.

Münchow, A. and R. W. Garvine. 1993a. Buoyancy and wind forcing of a coastal current. J. Mar. Res., *51*, 293–322.

—— 1993b. Dynamical properties of a buoyancy driven coastal current. J. Geophys. Res., *98*, 20,063–20,077.

Oke, P. R., J. S. Allen, R. N. Miller, G. D. Egbert, J. A. Austin, J. A. Barth, T. J. Boyd, P. M. Kosro and M. D. Levine. 2002. A modeling study of the three dimensional continental shelf circulation off Oregon. Part I: model-data comparisons. J. Phys. Oceanogr., *32*, 1360–1382.

Sanders, T. M. and R. W. Garvine. 1996. Frontal observations of the Delaware Coastal Current source region. Cont. Shelf Res., *16*, 1009–1021.

—— 2001. Fresh water delivery to the continental shelf and subsequent mixing: An observational study. J. Geophys. Res., *106*, 87–101.

Serway, R. A. and J. W. Jewett. 2004. Physics for Scientists and Engineers, 6th ed., Brooks/Cole Press, 330 pp.

Simpson, J. H. and D. G. Bowers. 1981. Models of stratification and frontal movement in shelf seas. Deep-Sea Res., *28*, 727–738.

Simpson, J. H., J. Brown, J. Matthews and G. Allen. 1990. Tidal straining, density currents, and stirring in the control of estuarine stratification. Estuaries, *13*, 125–132.

Simpson, J. H. and J. R. Hunter. 1974. Fronts in the Irish Sea. Nature, *250*, 404–406.

Simpson, J. H., J. Sharples and T. P. Rippeth. 1991. A prescriptive model of stratification induced by freshwater runoff. Estuar. Coast. Shelf Sci., *33*, 23–35.

Stommel, H. 1961. Thermohaline convection with two stable end regimes. Tellus, *13*, 224–230.
Whitney, M. M. and R. W. Garvine. 2005. Wind influence on a coastal buoyant outflow. J. Geophys. Res., *110*, 1–15.
—— 2006. Simulating the Delaware Bay outflow: Comparison with observations. J. Phys. Oceanogr., *36*, 3–21.
Wong, K. C. 1998. On the variability in the vertical structure of the Delaware Coastal Current. Cont. Shelf Res., *18*, 929–940.

Received: *7 June, 2008*; revised: *29 January, 2009*.